Electronic and optical properties of laterally composition-modulated $Al_xIn_{1-x}As$, $Ga_xIn_{1-x}P$, and $Ga_xIn_{1-x}As$ alloys

Yong Zhang and A. Mascarenhas
National Renewable Energy Laboratory, 1617 Cole Boulevard, Golden, Colorado 80401
(Received 5 January 1998)

Results of a systematic study of the band structure and optical properties of laterally-composition-modulated semiconductor alloys $Al_xIn_{1-x}As$, $Ga_xIn_{1-x}P$, and $Ga_xIn_{1-x}As$ are reported. [110] composition modulation occurs spontaneously during growth of (001) short-period superlattices or bulk epilayers of these alloys. The effect of this long-range lateral modulation is modeled using $\mathbf{k}\cdot\mathbf{p}$ theory and the envelope-function approximation, while the vertical short-period superlattice is emulated by a uniaxial perturbation. We have studied the dependence of the electronic and optical properties of such structures on the modulation amplitude, profile, and negative feedback due to the coherency strain field. We find that (i) among the three-alloy systems, for a given modulation amplitude, the largest band-gap reduction can be achieved in $Al_xIn_{1-x}As$, and the smallest in $Ga_xIn_{1-x}As$, (ii) a step-function modulation gives a larger band-gap reduction than a sinusoidal modulation; (iii) when the coherency strain is tetragonal in the modulated direction, a strong in-plane optical anisotropy is expected and when it is tetragonal in the growth direction, a weak in-plane optical anisotropy is anticipated; (iv) the vertical short-period superlattice enhances the band-gap reduction, but reduces the in-plane optical anisotropy; and (v) the lateral composition modulation is inherently associated with a diminishing of the vertical short-period superlattice. The possibility and conditions of type-II band alignment in these modulated structures are discussed. [S0163-1829(98)05519-2]

I. INTRODUCTION

Spontaneous lateral composition modulation (CM) has been observed in many III-V semiconductor alloys grown by either MBE (molecular beam epitaxy)[1–9] or MOVPE (metal-organic vapor-phase epitaxy).[10] Most research on CM has focused on three alloy systems: $Ga_xIn_{1-x}P$,[1–3,10] $Ga_xIn_{1-x}As$,[4–6] and $Al_xIn_{1-x}As$,[7–9] where the CM occurs along the [110] direction in the plane perpendicular to the [001] growth direction. The lateral CM has been observed to occur spontaneously when growing vertical short-period superlattice (SPS) structures,[1–6,9] although it has also been observed to occur during epitaxial growth of bulk alloys such as $Al_xIn_{1-x}As$ (Refs. 7, 8, and 10) and $Ga_xIn_{1-x}As$.[11]

Strained or unstrained [110] superlattices grown on (110) substrates have been modeled by using the $\mathbf{k}\cdot\mathbf{p}$ method in a number of previous studies.[12,13] However, those results are not applicable to laterally-composition-modulated structures, because of the coexistence of the vertical SPS or the strain coupling to the (001) substrate. There have been two attempts to model the electronic structure[2,14] and optical anisotropy[14] in laterally-composition-modulated $Ga_xIn_{1-x}P$. In Ref. 2, the effect of the CM is modeled by a lateral effective-mass superlattice of which the piecewise constant effective masses and band gaps in the Ga- or In-rich regions are calculated by diagnolizing the $\mathbf{k}\cdot\mathbf{p}$ Hamiltonians in each region. A similar approach has been used in Ref. 14 to model the anisotropy in the optical transitions. In both of these two previous studies, the band alignment between the Ga- and In-rich regions was type II (i.e., the topmost valence-band state was in the Ga-rich region while the lowest conduction-band state was in the In-rich region), which is an issue that needs further consideration. In this work, a more rigorous treatment of the problem will be given by using a multiband $\mathbf{k}\cdot\mathbf{p}$ Hamiltonian with a spatially varying effective potential tensor in which band-gap and strain-induced deformation potentials are modulated following the profile of the lateral CM.[15,16]

Experimentally, using photoluminescence studies, the band-gap reduction resulting from the lateral CM has been observed to be as large as $\sim$250 meV in MBE-grown $Ga_xIn_{1-x}P$,[17] $\sim$300 meV in MBE (Refs. 18 and 19) or MOCVD (Ref. 10) -grown $Al_xIn_{1-x}As$, and $\sim$100 meV in MBE-grown $Ga_xIn_{1-x}As$.[20,21] These values are roughly one order of magnitude larger than the band-gap reduction predicted for the corresponding SPS or CuAu-ordered structures.[22] Because of a lack of accurate knowledge in the amplitude of CM and its profile, and simplified theoretical approaches, quantitative comparisons of the optical anisotropy between the experimental results and theoretical expectations have not been satisfactory. Polarization anisotropy, defined as a ratio of the transition intensities polarized along directions perpendicular and parallel to the modulation, has been observed in a range of roughly 2–20 in different samples.[2,5,6,14,18,19,21]

The main purpose of this study is to achieve a better understanding of the dependence of band-gap reduction and optical anisotropy, on the various structural and material parameters, including variations in the modulation amplitude, modulation profile (step-function or sinusoidal), symmetry of the strain field, strength of vertical modulation, band offsets, and differences in alloy systems.

II. THEORETICAL MODELING

A. Qualitative consideration

We first consider the simplest situation in which the [110] oriented lateral CM occurs in a bulk alloy that has a

composition-independent lattice constant and is lattice-matched to the substrate. The properties of such a structure are essentially the same as that of a $GaAs/Al_xGa_{1-x}As$ superlattice grown on a (110) substrate. The difference is that the lateral superlattice exhibits a strong optical anisotropy in the growth plane, whereas the latter does not.

Next, we consider that in reality every one of the three-alloy systems, $Ga_xIn_{1-x}P$, $Al_xIn_{1-x}As$, and $Ga_xIn_{1-x}As$, has a composition-dependent lattice constant. Thus, because of the lateral CM, the epilayer will have a laterally-modulated-coherency strain field.[23,2] Depending on the epilayer thickness and the period of the modulation, the strain field can be very different.[23] When the epilayer is thin with respect to the modulation period, it is coherently strained by the substrate, and the distortion is tetragonal in the [001] growth direction; when the epilayer is thick with respect to the modulation period, in the region away from the substrate, laterally adjacent sheets strain each other, and the distortion is tetragonal in the [110] direction of the CM. In general, the strain is nonuniform along the growth direction, and evolves gradually from the thin-layer limit to the thick-layer limit. In reality, for a thick epilayer most optical measurements mainly probe the top portion of the epilayer. In this work, we will only consider these two extreme situations. In the case of thin epilayers, the tetragonal strain in the growth direction tends to reduce the in-pane anisotropy caused by the lateral CM, and so a relatively weak anisotropy is expected in the (001) growth plane. In the case of thick layers, the symmetry axis of the strain tensor is aligned with that of the modulation wave, and so the strong in-plane anisotropy is retained. In most published studies, typical modulation periods and epilayer thicknesses were found to be around 130–200 Å and 1000 Å,[2,9] respectively, making the thick-layer approximation more appropriate than the thin-layer one[23] for those cases. Although the primary cause for the lateral quantum confinement is the spatial variation of the band gap with the lateral CM, the coherency strain field plays an important role in determining the energy levels of the confined states. For the conduction band, the effect of strain tends to counterbalance the effect of pure composition variation, i.e., it reduces the well depth and barrier height, for both types of strain. For the valence band, the strain causes strong mixing of heavy- and light-hole states. The overall effect of the strain tends to diminish the band-gap reduction caused by pure CM, and this has been referred to earlier as the negative feedback effect.[2]

Finally, we consider the effect of the [001] SPS that is symmetrically equivalent to CuAu-ordering.[24] The major effects of ordering are well known as inducing a band-gap reduction and a valence-band splitting. The vertical SPS tends to enhance the band-gap reduction and weaken the in-plane anisotropy caused by the lateral CM. If an order parameter is defined as $\eta=1$ for an ideal vertical SPS,[24] the occurrence of the lateral CM will reduce the degree of order (i.e., $\eta<1$), because of swapping of cations between the A-rich and B-rich regions of the SPS $(AC)_m/(BC)_n$ $(m,n=1-2)$. This phenomenon has recently been confirmed by x-ray reciprocal space mapping experiments[25] in which the intensity of the vertical SPS diffraction spots is observed to decrease as the intensity of the diffraction spot due to the lateral CM increases. Figure 1 shows schematically two extreme situations: (a) the ideal vertical SPS with no CM ($\eta=1$), (b) 100% lateral CM with no SPS ($\eta=0$), and (c) a situation that is closer to reality: a partially modulated structure in which the vertical SPS is partially diminished due to lateral cation exchange.

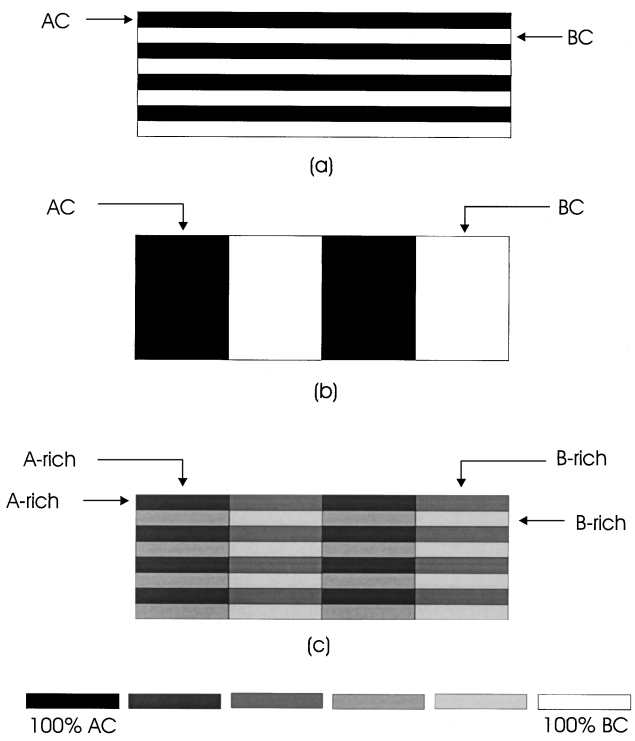

FIG. 1. Schematic diagrams showing (a) a vertical fully ordered short-period superlattice, (b) a lateral fully composition modulated superlattice, and (c) a partially ordered and partially modulated vertical and lateral superlattice.

B. Model

The composition-modulated structure is treated as a bulk alloy subjected to two perturbations: the lateral CM and the vertical SPS. The $\mathbf{k}\cdot\mathbf{p}$ Hamiltonian for the bulk alloy is given by $H_{\mathbf{k}\cdot\mathbf{p}}$ [Eq. (A1) in the Appendix]. When considering CM, we treat the unmodulated SPS $(AC)_m/(BC)_n$ as an alloy $A_{\bar{x}}B_{1-\bar{x}}C$ with an average composition $\bar{x}=m/(n+m)$. First, we describe the perturbation caused by the CM. The confinement potentials for the electron and hole generated by pure CM are determined by the conduction- and valence-band offsets. The unstrained band alignment between the A-rich and B-rich regions is chosen to be type I for the alloy systems considered in this work, with a ratio $Q_c=\Delta E_c/\Delta E_g=0.75$.[26] Although this value is not well established, we shall use it for our calculations. For the conduction band, the lateral confinement potential is defined as

$$V_e(z')=Q_c\{E_g[x(z')]-E_g(x_0)\}+a_c[\varepsilon_{xx}(z')+\varepsilon_{yy}(z')+\varepsilon_{zz}(z')], \quad (1)$$

where a_c is the conduction-band deformation potential, ε_{ij} is the strain tensor that will be defined later, and z' is along the direction of CM. For the valence band, the confinement potential is

$$V_h(z')=(1-Q_c)\{E_g[x(z')]-E_g(x_0)\}I+H_{\text{strain}}(z'), \tag{2}$$

where I is a 6×6 unit matrix, and H_{strain} is the strain potential [Eq. (A3) in the Appendix].

In a conventional cubic coordinate system with x, y, and z oriented along the [100], [010], and [001] directions, the strain tensor for the [001] tetragonal distortion is given as

$$\varepsilon_{xx}=\varepsilon_{yy}=\frac{a_0-a(x)}{a(x)},$$

$$\varepsilon_{zz}=-\varepsilon_{xx}\frac{2c_{12}}{c_{11}}, \tag{3}$$

$$\varepsilon_{xz}=\varepsilon_{zx}=\varepsilon_{yz}=\varepsilon_{zy}=\varepsilon_{xy}=\varepsilon_{yz}=0,$$

where $a(x)$ is the lattice constant of the bulk alloy $A_xB_{1-x}C$, $a_0=a(x_0)$ is the lattice constant at which the epilayer is lattice-matched to the substrate, and c_{ij} are elastic constants.

For the [110] tetragonal distortion, the strain tensor can be derived from a general theory given by Mailhiot and Smith.[27] The tensor we obtain is

$$\varepsilon_{zz}=\frac{a_0-\alpha(x)}{a(x)}\chi,$$

$$\varepsilon_{xx}=\varepsilon_{yy}=\varepsilon_{zz}\frac{2c_{44}-c_{12}}{2c_{44}+c_{11}+c_{12}}, \tag{4}$$

$$\varepsilon_{xy}=\varepsilon_{yx}=-\varepsilon_{zz}\frac{c_{11}+2c_{12}}{2c_{44}+c_{11}+c_{12}},$$

$$\varepsilon_{xz}=\varepsilon_{zx}=\varepsilon_{yz}=\varepsilon_{zy}=0,$$

where $\chi=2(\lambda-\xi)/\lambda$, λ is the modulation period and ξ is the width of the region with composition x. We have assumed that the composition variation is piecewise constant along the modulation direction. When $\xi=\lambda/2$, $\chi=1$, which leads to the strain tensor used in Refs. 2 and 14. If the composition variation is not piecewise constant but still symmetric, for instance, a sinusoidal variation, the above formulas are still applicable by setting $\chi=1$.

The [110] stain tensor given above looks complicated in the (x,y,z) coordinate system. Since its symmetry axis is the same as that of the CM, i.e., the [110] direction, we rewrite the strain tensor in a new coordinate system with z' along [110], x' along [001], and y' along [110]. It is then given as

$$\varepsilon_{x'x'}=\varepsilon_{y'y'}=\varepsilon_{zz},$$

$$\varepsilon_{z'z'}=\varepsilon_{xx}+\varepsilon_{xy}=\varepsilon_{zz}\frac{2c_{44}-c_{11}-3c_{12}}{2c_{44}+c_{11}+c_{12}}, \tag{5}$$

$$\varepsilon_{x'z'}=\varepsilon_{z'x'}=\varepsilon_{y'z'}=\varepsilon_{z'y'}=\varepsilon_{x'y'}=\varepsilon_{y'x'}=0.$$

Next, the effect of the vertical SPS can be emulated by a tetragonal distortion[28] or CuAu ordering.[24] The perturbative Hamiltonian in the conventional basis can be written as[24]

$$H_{\text{SPS}}=-\frac{\Delta_{\text{CF}}}{3}\begin{pmatrix}1&0&0&0&0&0\\0&-1&0&0&\sqrt{2}&0\\0&0&-1&0&0&\sqrt{2}\\0&0&0&1&0&0\\0&\sqrt{2}&0&0&0&0\\0&0&\sqrt{2}&0&0&0\end{pmatrix}, \tag{6}$$

where Δ_{CF} is the crystal-field-splitting parameter. For perfectly ordered $(GaP)_1/(InP)_1$, $(GaAs)_1/(InAs)_1$, and $(AlAs)_1/(InAs)_1$ superlattices, Δ_{CF} is predicted to be 191, 134, and 270 meV, respectively.[22] The crystal-field splitting contributes to the band-gap reduction by an amount $\Delta_{\text{CF}}/3$, which for CuAu ordering represents most of the ordering-induced band-gap reduction.[22] Thus, we can ignore other contributions to the band-gap reduction due to the CuAu ordering. As mentioned earlier, the CM effectively reduces the degree of order of the vertical SPS because of lateral cation exchange. If the modulation amplitude is assumed to be δx, the maximum value possible for the CuAu order parameter will be[29]

$$\eta(\delta x)=\min[2(x_0+\delta x),2(1-x_0-\delta x)], \tag{7}$$

where min means that $\eta(\delta x)$ is the smaller value of $2(x_0+\delta x)$ and $2(1-x_0-\delta x)$. The η dependence of the crystal-field-splitting parameter can be written as[24]

$$\Delta_{\text{CF}}[\eta(\delta x)]=\eta^2\Delta_{\text{CF}}(\eta=1). \tag{8}$$

The conduction band is treated by a one-band model with an isotropic effective mass and a confinement potential given by Eq. (1). For the valence band, the total Hamiltonian is the sum of $H_{\mathbf{k}\cdot\mathbf{p}}$, Eq. (2), and Eq. (6). The band structure of the composition modulated structure can be obtained by using the envelope-function approximation.[30,15] In our calculation, the $\mathbf{k}\cdot\mathbf{p}$ Hamiltonian in the conventional basis with its quantization axis along the [001] direction has been transformed to that in a new basis with its quantization axis along the z' direction (for both angular momentum and spin) and in the new coordinate system (x',y',z'). Details are given in the Appendix. In the new basis, Eq. (6) becomes

TABLE I. Material parameters for the three-alloy systems used in our calculations.

Parameter (units)	$Al_xIn_{1-x}As$	$Ga_xIn_{1-x}P$	$Ga_xIn_{1-x}As$
E_g (eV)	$0.43+2.6x+0.633\ x\ (x-1)$	$1.424+1.46x+0.76\ x\ (x-1)$	$0.43+1.087x+0.460\ x\ (x-1)$
Δ_{so} (eV)	$0.38-0.105x$	$0.11-0.03x-0.035x\ (x-1)$	$0.38-0.039x$
E_p (eV)	$21.1x+21.11\ (1-x)$	$31.4x+20.7\ (1-x)$	$22.71x+21.11\ (1-x)$
γ_1	$4.04x+20.4\ (1-x)$	$4.05x+5.05\ (1-x)$	$6.8x+20.4\ (1-x)$
γ_2	$0.78x+8.3\ (1-x)$	$0.49x+1.6\ (1-x)$	$1.9x+8.3\ (1-x)$
γ_3	$1.57x+9.1\ (1-x)$	$1.25x+1.73\ (1-x)$	$2.73x+9.1\ (1-x)$
a_c (eV)	$-5.64x-5.08\ (1-x)$	$-7.14x-5.04\ (1-x)$	$-7.17x-5.08\ (1-x)$
a (eV)	$2.47x+1.00\ (1-x)$	$1.7x+1.27\ (1-x)$	$1.16x+1.00\ (1-x)$
b (eV)	$-1.5x-1.55\ (1-x)$	$-1.4x-1.55\ (1-x)$	$-1.9x-1.55\ (1-x)$
d (eV)	$-3.4x-3.10\ (1-x)$	$-4.5x-4.2\ (1-x)$	$-4.23x-3.10\ (1-x)$
c_{11} (10^{11} dyn/cm^2)	$12.02x+8.329\ (1-x)$	$14.387x+10.22\ (1-x)$	$11.88x+8.329\ (1-x)$
c_{12} (10^{11} dyn/cm^2)	$5.70x+4.526\ (1-x)$	$6.520x+5.76\ (1-x)$	$5.38x+4.526\ (1-x)$
c_{44} (10^{11} dyn/cm^2)	$5.89x+3.959\ (1-x)$	$7.143x+4.60\ (1-x)$	$5.94x+3.959\ (1-x)$
$a(x_0)$ (Å)	5.8658	5.6480	5.8658

$$H'_{\mathrm{SPS}}=\frac{\Delta_{\mathrm{CF}}}{3}\begin{pmatrix} \frac{1}{2} & 0 & \frac{\sqrt{3}}{2} & 0 & 0 & \sqrt{\frac{3}{2}} \\ 0 & -\frac{1}{2} & 0 & -\frac{\sqrt{3}}{2} & \frac{1}{\sqrt{2}} & 0 \\ \frac{\sqrt{3}}{2} & 0 & -\frac{1}{2} & 0 & 0 & \frac{1}{\sqrt{2}} \\ 0 & -\frac{\sqrt{3}}{2} & 0 & \frac{1}{2} & -\sqrt{\frac{3}{2}} & 0 \\ 0 & \frac{1}{\sqrt{2}} & 0 & -\sqrt{\frac{3}{2}} & 0 & 0 \\ \sqrt{\frac{3}{2}} & 0 & \frac{1}{\sqrt{2}} & 0 & 0 & 0 \end{pmatrix}. \tag{9}$$

Spatial dependence of the material parameters (Luttinger parameters, deformation potentials, and elastic constants, etc.) has been taken into account.

C. Numerical results

We consider two types of CM profiles: step function and sinusoidal. We define the spatially dependent composition $x(z')$ as

$$x(z')=x_0+\delta x_0+\delta x(z'), \tag{10}$$

where x_0 is the composition at which the lattice constant of the epilayer matches that of the substrate, δx_0 is the deviation of the average composition from x_0, and $\delta x(z')$ is the spatially dependent part of the deviation. For the alloy $A_xB_{1-x}C$, if the CM profile is step-function-like, the A-rich region has a modulation amplitude $\delta x_A>0$ with a width l_A and the B-rich region has a modulation amplitude $\delta x_B<0$ with a width l_B, the relation $\delta x_A l_A+\delta x_B l_B=0$ has to be satisfied. For a sinusoidal distribution, we write $\delta x(z')=\delta x\cos(2\pi z'/L)$, where δx is the modulation amplitude, L is the period, and $z'=0$ is chosen as the center of the A-rich region. Band structure and material parameters used in our calculations are listed in Table I.

All the numerical results shown in this section are for the lateral strain modulation corresponding to a tetragonal distortion along the [110] direction. In the next section, we will briefly discuss the results for the CM in thin epilayers where the tetragonal distortion occurs along the [001] direction.

First, we consider the band-gap change as a function of CM amplitude. We assume that the modulation period is 200 Å, the profile is step-function-like, symmetric (i.e., $l_A=l_B$), and with an amplitude δx. For simplicity, we assume $\delta x_0=0$ (i.e., the epilayer is lattice-matched to the substrate at its

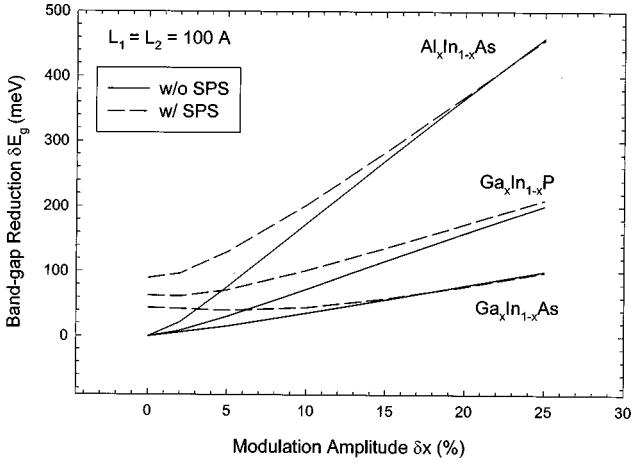

FIG. 2. Band-gap reduction as a function of composition-modulation amplitude for the three-alloy systems, with and without the vertical short-period superlattice.

average composition). For the lateral strain modulation corresponding to a [110] tetragonal distortion, Fig. 2 shows band-gap reductions as a function of δx for the three-alloy systems, with and without the presence of the SPS. There are two major observations: (i) for a given modulation amplitude, the band-gap reduction is largest in $Al_xIn_{1-x}As$ and smallest in $Ga_xIn_{1-x}As$; (ii) the SPS causes an enhancement in the band-gap reduction, but this effect diminishes with increasing CM amplitude.

Second, we consider the optical anisotropy caused by the CM. Figure 3 shows the intensity (square of the transition matrix element) for the transition between the first conduction and valence subbands as a function of δx for the three-alloy systems, with and without the SPS. Without the SPS, the lateral CM makes the topmost valence-band states $|3/2,\pm 3/2\rangle_{[110]}$-like. The transitions are forbidden for light polarized along [110], and allowed for light polarized along [110]. However, because the [110] tetragonal distortion occurs along a low symmetry axis and the valence-band structure is complex (i.e., $\gamma_2 \neq \gamma_3$), the [110] polarization is not perfectly forbidden, but the polarization ratio between the [110] and [110] is a large number, typically greater than 100. Thus, a very strong optical anisotropy is expected for a bulk sample with lateral CM, although the excitonic effect tends to further enhance the forbidden transition and so reduce the anisotropy.[31] With the coexistence of the SPS, the situation can be very different. When the CM is relatively weak so that the SPS effect is dominant, the topmost valence-band states are $|3/2,\pm 3/2\rangle_{[001]}$-like, and both of the [110] and [110] polarizations are allowed. However, the lateral CM causes the [110] polarization to be stronger than that of the [110] polarization. When the lateral CM becomes dominant, the [110] polarization becomes nearly forbidden. The numerical results are shown in Figs. 3(a)–3(c).

Until now, accurate measurements of the amplitude, profile, and period of the modulation still remain technically difficult or impractical due to sample quality. For the $Ga_xIn_{1-x}P$ sample studied in Ref. 2, the period was estimated to be 200 Å, and the composition variation was estimated to range from 44% to 58%. A band-gap reduction of

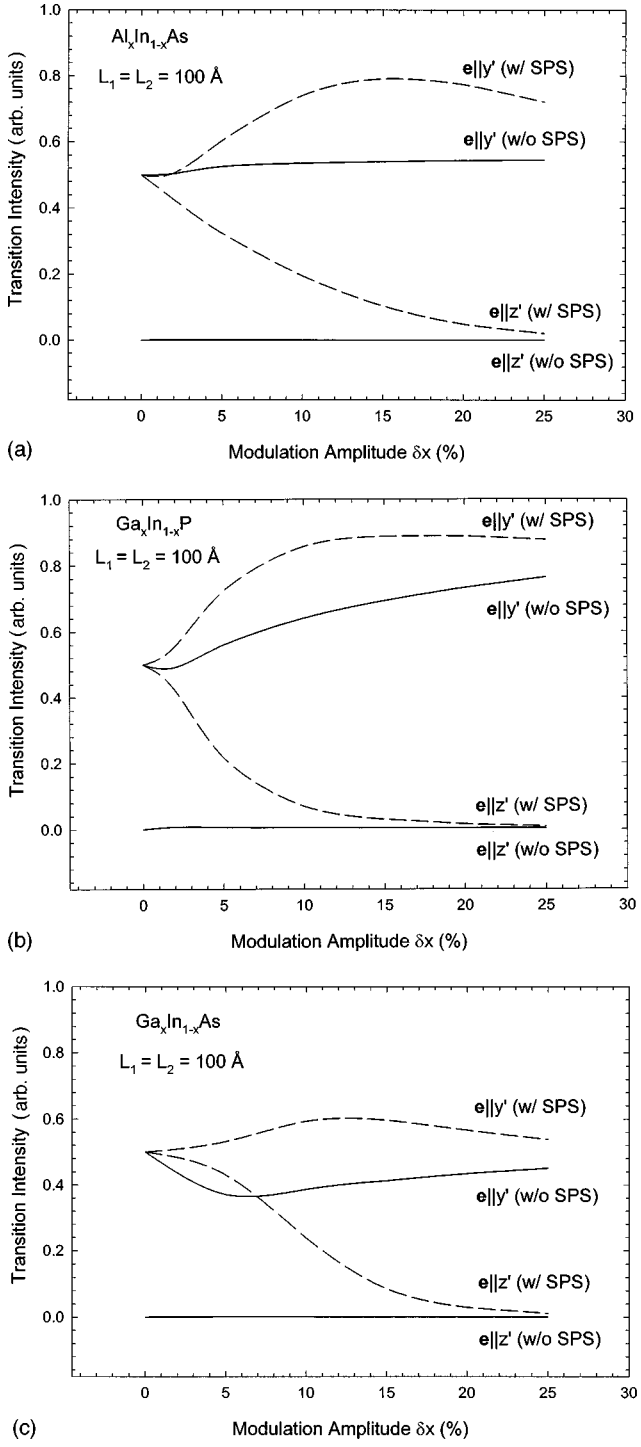

FIG. 3. Optical transition intensity as a function of composition-modulation amplitude for polarizations $y' \sim [110]$ and $z' \sim [110]$, with and without the vertical short-period superlattice. (a) $Al_xIn_{1-x}As$, (b) $Ga_xIn_{1-x}P$, and (c) $Ga_xIn_{1-x}As$.

~ 140 meV and a polarization ratio of 7 ± 1 were observed in this particular sample. Assuming the [110] tetragonal distortion and the step-function-like modulation profile, and using the given estimated parameters, we have calculated the band-gap reduction and the polarization ratio to be 93 meV and 7.7, assuming the maximum possible order parameter for the SPS coexisting with CM. Without the SPS, these values would be 57 meV and 104.

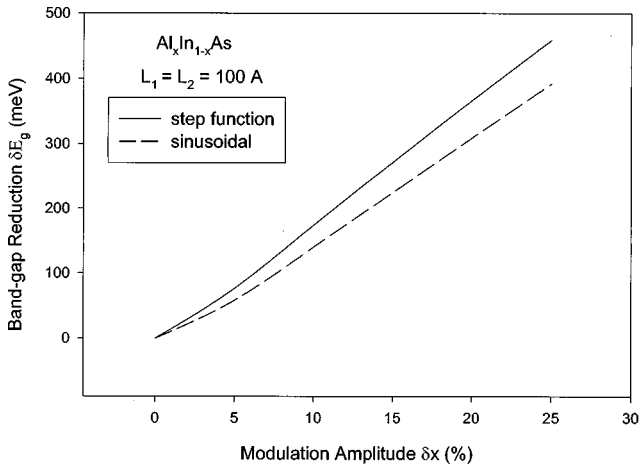

FIG. 4. Comparison of band-gap reductions with step function and sinusoidal modulations.

Next, we consider the effects due to the difference in the modulation profile. Figure 4 shows the comparison in band-gap reductions as a function of modulation amplitude for $Al_xIn_{1-x}As$. Comparing a sinusoidal to a step-function-like CM profile for the same modulation amplitude, we get a smaller band-gap reduction with the sinusoidal distribution. This is due to the fact that the quantum confinement energy is larger in a sinusoidal potential well due to the smaller effective well width.

III. DISCUSSIONS

As shown in Fig. 2, for a given modulation amplitude, the $Al_xIn_{1-x}As$ system has the largest band-gap reduction among the three-alloy systems, with and without the vertical SPS. Without the vertical SPS, the two major causes of the difference in the magnitude of the band-gap reduction are the rate of band-gap change with composition change near x_0, and the conduction-band effective mass. The former is critical in determining the depth of the well and the height of the barrier, the latter being the major parameter that determines the confinement energy of the particle. The rate of the band-gap change is roughly proportional to the band-gap difference between the two binary compounds, if bowing is not too strong. Thus, we expect to have the largest band-gap reduction in the $Al_xIn_{1-x}As$ system, since the difference in the direct gaps $E_g(\mathrm{AlAs})-E_g(\mathrm{InAs})=2.6$ eV, $E_g(\mathrm{GaP})-E_g(\mathrm{InP})=1.46$ eV, and $E_g(\mathrm{GaAs})-E_g(\mathrm{InAs})=1.09$ eV. On the other hand, $Ga_xIn_{1-x}As$ has the smallest conduction-band effective mass, which gives a large electron confinement energy, and therefore a small contribution to the band-gap reduction. These two considerations explain the sequence of band-gap reductions among the three-alloy systems. Even with the SPS, the sequence does not change, since Δ_{CF} is largest in $Al_xIn_{1-x}As$ and smallest in $Ga_xIn_{1-x}As$. It is worth pointing out that the SPS does not always enhance the band-gap reduction. As shown by the curves in Fig. 2 for $Ga_xIn_{1-x}As$, in the strongly modulated case, the band-gap reduction is smaller with the SPS than without it, which is because of the strong coupling between the vertical SPS and the lateral modulation on the valence bands and the relatively small contribution from the conduction-band edge in $Ga_xIn_{1-x}As$.

As regards optical anisotropy, these three systems are qualitatively similar in the strongly modulated regime. In general, the polarization is more sensitive to the symmetry change than the numerical difference in material parameters. However, in the weakly modulated region, the detailed balance among different perturbations does make the difference among the three systems more significant. The vertical SPS can significantly reduce the in-plane optical anisotropy caused by the pure lateral CM, while the [110] tetragonal distortion has very little effect on the anisotropy.

For thin epilayers where the CM corresponds to a [001] tetragonal distortion, the band-gap reduction is slightly larger than the situations for the [110] tetragonal distortion shown in Fig. 2 (typically by $\sim 10\%$ without the SPS). The more important difference from the [110] tetragonal distortion is that a much weaker in-plane optical anisotropy (typically a ratio of ~ 3) is found with the [001] tetragonal distortion, which is a result of the strong interaction between the two perpendicular perturbations: the in-plane biaxial strain and the lateral CM. This may explain the small optical anisotropy observed in a few earlier studies.[5,6,14]

Next, we discuss the competitions among the pure lateral CM, coherency strain, and vertical SPS. For the conduction band, the band-edge shifts due to the pure lateral CM and coherency strain tend to have a counterbalancing effect, as pointed out in Ref. 2 as being the result of negative feedback. Unless Q_c is unusually small, the In-rich region has a lower band-edge energy than the Al- (or Ga-) rich region. The effect of the negative feedback is stronger for the [110] tetragonal distortion than that for the [001] tetragonal distortion, since the traces of the strain tensors are $\mathrm{Tr}(\varepsilon)\approx 7/5\,\varepsilon_0$ and ε_0, respectively, for the two situations, where $\varepsilon_0=[a_0-a(x)]/a(x)$ (in cubic alloys, $c_{11}\approx 2c_{12}$ and $c_{12}\approx c_{44}$).

For the valence band, the coherency strain more or less has the same effect as for the conduction band, but in a more complicated way. Let us consider the situation with the [110] tetragonal distortion. We can split the band-edge shifts of the valence-band states into three contributions:

$$\delta E_v=\delta E_v(x)+\delta E_v(\varepsilon,\mathrm{hydro})+\delta E_v(\varepsilon,\mathrm{shear/sps}), \tag{11}$$

where $\delta E_v(x)$ is the contribution of pure CM, $\delta E_v(\varepsilon,\mathrm{hydro})$ is due to hydrostatic strain, and $\delta E_v(\varepsilon,\mathrm{shear/sps})$ is the contribution of shear strain and the vertical SPS. To illustrate the basic physics more clearly, we use a four-band approximation, i.e., assuming a large spin-orbit splitting. For the topmost valence-band edge, $\delta E_{v1}(\varepsilon,\mathrm{shear/sps})=-\sqrt{\bar{q}^2+\bar{r}^2+q_0^2-q_0(\bar{q}+\sqrt{3}\bar{r})}$, and the second valence-band edge, $\delta E_{v2}(\varepsilon,\mathrm{shear/sps})=\sqrt{\bar{q}^2+\bar{r}^2+q_0^2-q_0(\bar{q}+\sqrt{3}\bar{r})}$, where $q_0=\Delta_{\mathrm{CF}}/3$, $\bar{q}$ and $\bar{r}$ are related to shear strain (defined in the Appendix). Without the SPS (i.e., $q_0=0$), the band offset between the In-rich and Al- (or Ga-) rich regions is approximately $E_{\mathrm{VBO}}=2[|\delta E_v(x)|-|\delta E_v(\varepsilon,\mathrm{hydro})|]$. If $E_{\mathrm{VBO}}>0$, the highest valence-band edge is in the In-rich region, so the band alignment is type I. For the band-offset ratio $Q_c=75\%$, all three-alloy systems have a type-I alignment. With the SPS, the contributions of the shear terms in

the band offset do not cancel each other, which, in fact, reduces the band offset. For all three alloys, the band alignment remains as type I for the assumed $Q_c = 75\%$. A new solar cell structure based on the type-II alignment in a composition-modulated structure has been proposed recently.[32] To achieve this goal, an alloy system with a small composition variation of the band gap, a large hydrostatic deformation potential, and a strong CuAu ordering is advantageous. Of course, a system with unstrained type-II alignment would be most desirable. If the coupling to the spin-orbit split-off band is taken into account, a small Δ_{SO} is of help in achieving the type-II alignment, because the coupling pushes the $|3/2,\pm 1/2\rangle$-like states up toward the conduction band in the Al- (or Ga-) rich region in the three alloys considered.

IV. SUMMARY

We have conducted a systematic study of the band structures and optical anisotropy of spontaneous laterally composition modulated semiconductor alloys: $Al_xIn_{1-x}As$, $Ga_xIn_{1-x}P$, and $Ga_xIn_{1-x}As$. We have focused on the competition between composition modulation and the negative feedback effect of coherency strain in determining the Brillouin-zone center electronic and optical properties. In this study, we have specifically accounted for the fact that as the amplitude of the spontaneous lateral composition modulation increases, the order parameter of the artificially grown vertical short-period superlattice decreases.

A summary of the major results is as follows.

(i) Among the three alloy systems, for a given modulation amplitude, a largest band-gap reduction can be achieved in $Al_xIn_{1-x}As$, and the smallest in $Ga_xIn_{1-x}As$.

(ii) For a given alloy system, a step-function modulation gives a larger band-gap reduction than a sinusoidal modulation.

(iii) In a relatively thick epilayer in which the coherency strain field is approximately tetragonal in the direction of CM, a strong in-plane optical anisotropy is expected, while in a relatively thin epilayer in which the coherency strain field is approximately tetragonal in the direction of the growth, a weak in-plane optical anisotropy is anticipated.

(iv) A vertical short-period superlattice enhances the band-gap reduction for weak composition modulations, and reduces the in-plane optical anisotropy.

(v) The lateral CM causes a weakening in the vertical CuAu ordering. In weakly modulated structures, the vertical short-period superlattice plays an important role in the electronic and optical properties. However, in the strongly modulated structures, the effects of the vertical short-period superlattice are rather weak.

(vi) The valence-band offset is mainly determined by the difference between the contributions of the composition dependence of the band gap and the hydrostatic term of the strain field, when there is no vertical short-period superlattice and with a large spin-orbit interaction. With the vertical short-period superlattice, the shear strain also contributes to the band offset.

ACKNOWLEDGMENTS

This work was supported by the U.S. Office of Energy Research, Material Science Division of DOE under Contract No. DE-AC36-83CH10093.

APPENDIX

The $\mathbf{k}\cdot\mathbf{p}$ Hamiltonians are taken from Ref. 16. In the conventional basis $\mathbf{u}=\{|3/2,-3/2\rangle_{[001]},|3/2,-1/2\rangle_{[001]}, |3/2,1/2\rangle_{[001]},|3/2,3/2\rangle_{[001]}, |1/2,-1/2\rangle_{[001]}, |1/2,1/2\rangle_{[001]}\}$ and the coordinate system with z along [001], x along [100], and y along [010], the $\mathbf{k}\cdot\mathbf{p}$ Hamiltonian for the valence band is given as

$$H_{\mathbf{k}\cdot\mathbf{p}} = -\begin{pmatrix} -P+Q & S^* & R^* & 0 & -\frac{1}{\sqrt{2}}S'^* & \sqrt{2}R'^* \\ S & -P-Q & 0 & -R^* & \sqrt{2}Q' & \sqrt{\frac{3}{2}}S'^* \\ R & 0 & -P-Q & S^* & -\sqrt{\frac{3}{2}}S' & \sqrt{2}Q' \\ 0 & -R & S & -P+Q & -\sqrt{2}R' & -\frac{1}{\sqrt{2}}S' \\ -\frac{1}{\sqrt{2}}S' & \sqrt{2}Q' & -\sqrt{\frac{3}{2}}S'^* & -\sqrt{2}R'^* & Z & 0 \\ \sqrt{2}R' & \sqrt{\frac{3}{2}}S' & \sqrt{2}Q' & -\frac{1}{\sqrt{2}}S'^* & 0 & Z \end{pmatrix}, \tag{A1}$$

with

$$P=\frac{\hbar^2}{2m}\,\gamma_1(k_1^2+k_2^2+k_3^2),$$

$$Q=-\frac{\hbar^2}{2m}\,\gamma_2(k_1^2+k_2^2-2k_3^2),$$

$$R=-\sqrt{3}\,\frac{\hbar^2}{2m}\,[\gamma_2(k_1^2-k_2^2)-2i\gamma_3k_1k_2],$$

$$S=2\sqrt{3}\,\frac{\hbar^2}{2m}\,\gamma_3k_3(k_1-ik_2),$$

$$Z=-\Delta_{so}-\frac{\hbar^2}{2m}\,\gamma_1'(k_1^2+k_2^2+k_3^2),$$

$$Q'=-\frac{\hbar^2}{2m}\,\gamma_2'(k_1^2+k_2^2-2k_3^2),$$

$$R'=-\sqrt{3}\,\frac{\hbar^2}{2m}\,[\gamma_2'(k_1^2-k_2^2)-2i\gamma_3'k_1k_2],$$

$$S'=2\sqrt{3}\,\frac{\hbar^2}{2m}\,\gamma_3'k_3(k_1-ik_z),$$

(A2)

where γ_1, γ_2, and γ_3 are Luttinger parameters, $\gamma_1'=\gamma_1+E_p/3\ (1/E_d-1/E_g)$, $\gamma_2'=\gamma_2+E_p/12\ (1/E_d-1/E_g)$, $\gamma_3'=\gamma_3+E_p/12\ (1/E_d-1/E_g)$, $E_d=E_g+\Delta_{so}$, E_p is a constant related to the transition matrix element.

The perturbative Hamiltonian associated with strain is given as

$$H_{\text{strain}}=-\begin{pmatrix} -p+q & s^* & r^* & 0 & -\frac{1}{\sqrt{2}}s'^* & \sqrt{2}r'^* \\ s & -p-q & 0 & -r^* & \sqrt{2}q' & \sqrt{\frac{3}{2}}s'^* \\ r & 0 & -p-q & s^* & -\sqrt{\frac{3}{2}}s' & \sqrt{2}q' \\ 0 & -r & s & -p+q & -\sqrt{2}r' & -\frac{1}{\sqrt{2}}s' \\ -\frac{1}{\sqrt{2}}s' & \sqrt{2}q' & -\sqrt{\frac{3}{2}}s'^* & -\sqrt{2}r'^* & z & 0 \\ \sqrt{2}r' & \sqrt{\frac{3}{2}}s' & \sqrt{2}q' & -\frac{1}{\sqrt{2}}s'^* & 0 & z \end{pmatrix}, \tag{A3}$$

with

$$p=-a_1(\varepsilon_{xx}+\varepsilon_{yy}+\varepsilon_{zz}),$$

$$q=\frac{b_1}{2}\,(\varepsilon_{xx}+\varepsilon_{yy}-2\varepsilon_{zz}),$$

$$r=\frac{\sqrt{3}b_1}{2}\,(\varepsilon_{xx}-\varepsilon_{yy})-id_1\varepsilon_{xy},$$

$$s=-d_1(\varepsilon_{xz}-i\varepsilon_{yz}),$$

$$z=a_2(\varepsilon_{xx}+\varepsilon_{yy}+\varepsilon_{zz}),$$

$$q'=\frac{b_2}{2}\,(\varepsilon_{xx}+\varepsilon_{yy}-2\varepsilon_{zz}),$$

$$r'=\frac{\sqrt{3}b_2}{2}\,(\varepsilon_{xx}-\varepsilon_{yy})-id_2\varepsilon_{xy},$$

$$s'=-d_2(\varepsilon_{xz}-i\varepsilon_{yz}),$$

(A4)

where $a_1=a+\delta a$, $b_1=b+2\delta b$, $d_1=d+2\delta d$, $a_2=a-2\delta a$, $b_2=b-\delta b$, $d_2=d-\delta d$, a, b, and d are deformation potentials for the valence band defined by Bir and Pikus,[33] $\delta a=-2\Delta_{so}/9$, $\delta b=-\Delta_{so}/9$, and $\delta d=-\sqrt{3}\Delta_{so}/9$ are corrections to the spin-orbit interaction due to the effect of strain.[34]

Now we would like to transform Hamiltonians (A1) and (A3) to a new basis $\mathbf{u}'=\{|3/2,-3/2\rangle_{[110]},|3/2,-1/2\rangle_{[110]},|3/2,1/2\rangle_{[110]},\ |3/2,3/2\rangle_{[110]},\ |1/2,\ -1/2\rangle_{[110]},|1/2,1/2\rangle_{[110]}\}$ and in a new coordinate system with z' along [110], x' along [001], and y' along [110]. The coordinate transform is chosen as

$$\begin{pmatrix} x' \\ y' \\ z' \end{pmatrix}=\begin{pmatrix} 0 & 0 & 1 \\ \frac{1}{\sqrt{2}} & -\frac{1}{\sqrt{2}} & 0 \\ \frac{1}{\sqrt{2}} & \frac{1}{\sqrt{2}} & 0 \end{pmatrix}\begin{pmatrix} x \\ y \\ z \end{pmatrix}. \tag{A5}$$

The transformation of spin is realized by

$$\begin{pmatrix} \uparrow' \\ \downarrow' \end{pmatrix} = \begin{pmatrix} e^{-i\phi/2}\cos(\theta/2) & e^{i\phi/2}\sin(\theta/2) \\ -e^{-i\phi/2}\sin(\theta/2) & e^{i\phi/2}\cos(\theta/2) \end{pmatrix} \begin{pmatrix} \uparrow \\ \downarrow \end{pmatrix}, \quad \text{(A6)}$$

where $\theta = 90°$ and $\phi = 45°$.

With Eqs. (A5) and (A6), the Hamiltonians can be transformed accordingly from basis $\mathbf{u}$ to $\mathbf{u}'$. However, in the basis $\mathbf{u}'$, the spin-orbit interaction term is nondiagonal. We then applied another transformation to diagonalize the spin-orbit interaction term:

$$\begin{aligned} u_2'' &= -\tfrac{1}{3}|3/2,-1/2\rangle_{[110]} + \frac{2\sqrt{2}}{3}|1/2,-1/2\rangle_{[110]}, \\ u_5'' &= \frac{2\sqrt{2}}{3}|3/2,-1/2\rangle_{[110]} + \frac{1}{3}|1/2,-1/2\rangle_{[110]}, \\ u_3'' &= -\tfrac{1}{3}|3/2,1/2\rangle_{[110]} + \frac{2\sqrt{2}}{3}|1/2,1/2\rangle_{[110]}, \\ u_6'' &= \frac{2\sqrt{2}}{3}|3/2,1/2\rangle_{[110]} + \tfrac{1}{3}|1/2,1/2\rangle_{[110]}, \\ u_1'' &= |3/2,-3/2\rangle_{[110]}, \\ u_4'' &= |3/2,3/2\rangle_{[110]}. \end{aligned} \quad \text{(A7)}$$

The Hamiltonians (A1) and (A3) in the basis $\mathbf{u}''$ presented in the same format as in Eqs. (A1) and (A3) have the following matrix elements:

$$\begin{aligned} \overline{P} &= \frac{\hbar^2}{2m}\gamma_1(k_1'^2 + k_2'^2 + k_3'^2), \\ \overline{Q} &= \frac{\hbar^2}{2m}[\tfrac{1}{2}\gamma_2(k_2'^2 + k_3'^2 - 2k_1'^2) + \tfrac{3}{2}\gamma_3(k_3'^2 - k_2'^2)], \\ \overline{R} &= \frac{\sqrt{3}}{2}\frac{\hbar^2}{2m}[\gamma_2(k_2'^2 + k_3'^2 - 2k_1'^2) + \gamma_3(k_2'^2 - k_3'^2 + 4ik_1'k_2')], \\ \overline{S} &= -2\sqrt{3}\frac{\hbar^2}{2m}k_3'(\gamma_3 k_1' - i\gamma_2 k_2'), \\ \overline{Z} &= -\Delta_{so} - \frac{\hbar^2}{2m}\gamma_1'(k_1'^2 + k_2'^2 + k_3'^2), \\ \overline{Q'} &= \frac{\hbar^2}{2m}[\tfrac{1}{2}\gamma_2'(k_2'^2 + k_3'^2 - 2k_1'^2) + \tfrac{3}{2}\gamma_3'(k_3'^2 - k_2'^2)], \\ \overline{R'} &= \frac{\sqrt{3}}{2}\frac{\hbar^2}{2m}[\gamma_2'(k_2'^2 + k_3'^2 - 2k_1'^2) + \gamma_3'(k_2'^2 - k_3'^2 + 4ik_1'k_2')], \\ \overline{S'} &= -2\sqrt{3}\frac{\hbar^2}{2m}k_3'(\gamma_3'k_1' - i\gamma_2'k_2'), \end{aligned} \quad \text{(A8)}$$

$$\begin{aligned} \overline{p} &= -a_1(\varepsilon_{x'x'} + \varepsilon_{y'y'} + \varepsilon_{z'z'}), \\ \overline{q} &= -\tfrac{1}{4}[b_1(\varepsilon_{y'y'} + \varepsilon_{z'z'} - 2\varepsilon_{x'x'}) + \sqrt{3}d_1(\varepsilon_{z'z'} - \varepsilon_{y'y'})], \\ \overline{r} &= -\tfrac{1}{4}[\sqrt{3}b_1(\varepsilon_{y'y'} + \varepsilon_{z'z'} - 2\varepsilon_{x'x'}) + d_1(\varepsilon_{y'y'} - \varepsilon_{z'z'} + i4\varepsilon_{x'y'})], \\ \overline{s} &= d_1\varepsilon_{x'z'} - i\sqrt{3}b_1\varepsilon_{y'z'}, \\ \overline{z} &= a_2(\varepsilon_{x'x'} + \varepsilon_{y'y'} + \varepsilon_{z'z'}), \\ \overline{q'} &= -\tfrac{1}{4}[b_2(\varepsilon_{y'y'} + \varepsilon_{z'z'} - 2\varepsilon_{x'x'}) + \sqrt{3}d_2(\varepsilon_{z'z'} - \varepsilon_{y'y'})], \\ \overline{r'} &= -\tfrac{1}{4}[\sqrt{3}b_2(\varepsilon_{y'y'} + \varepsilon_{z'z'} - 2\varepsilon_{x'x'}) + d_2(\varepsilon_{y'y'} - \varepsilon_{z'z'} + i4\varepsilon_{x'y'})], \\ \overline{s'} &= d_2\varepsilon_{x'z'} - i\sqrt{3}b_2\varepsilon_{y'z'}. \end{aligned} \quad \text{(A9)}$$

[1] K. C. Hsieh, J. N. Baillargeon, and K. Y. Cheng, Appl. Phys. Lett. **57**, 2244 (1990).

[2] A. Mascarenhas, R. G. Alonso, G. S. Horner, S. Froyen, K. C. Hsieh, and K. Y. Cheng, Superlattices Microstruct. **12**, 57 (1992); A. Mascarenhas, R. G. Alonso, G. S. Horner, and S. Froyen, Phys. Rev. B **48**, 4907 (1993).

[3] A. C. Chen, A. M. Moy, P. J. Pearah, K. C. Hsieh, and K. Y. Cheng, Appl. Phys. Lett. **62**, 1359 (1993).

[4] K. Y. Cheng, K. C. Hsieh, and J. N. Baillargeon, Appl. Phys. Lett. **60**, 2892 (1992).

[5] S. T. Chou, K. C. Hsieh, K. Y. Cheng, and L. J. Chou, J. Vac. Sci. Technol. B **13**, 650 (1995).

[6] S. T. Chou, K. Y. Cheng, L. J. Chou, and K. C. Hsieh, Appl. Phys. Lett. **66**, 2220 (1995).

[7] F. Peiro, A. Cornet, J. C. Ferrer, J. R. Morante, G. Halkias, and A. Georgakilas, in *Optoelectronic Materials—Ordering, Composition Modulation, and Self-Assembled Structures*, edited by E. D. Jones, A. Mascarenhas, P. Petroff, and R. Bhat, MRS Symposia Proceedings No. 417 (Materials Research Society, Pittsburgh, 1996), p. 265.

[8] E. Bearzi, T. Benyattou, C. Bru-chevallier, G. Guillot, J. C. Harmand, O. Marty, and M. Pitaval (Ref. 7), p. 271.

[9] J. Mirecki Millunchick, R. D. Twesten, D. M. Follstaedt, S. R. Lee, E. D. Jones, Yong Zhang, H. M. Cheong, S. P. Ahrenkiel, and A. Mascarenhas, Appl. Phys. Lett. **70**, 1402 (1997).

[10] S. W. Jun, T.-Y. Seong, J. H. Lee, and B. Lee, Appl. Phys. Lett. **68**, 3443 (1996).

[11] R. D. Twesten, D. M. Follstaedt, E. J. Heller, E. D. Jones, S. R. Lee, J. Mirecki Millunchick, F. A. J. M. Driessen, J. D. Perkins, and A. Mascarenhas, Bull. Am. Phys. Soc. **41**, 693 (1996).

[12] J. Los, A. Fasolino, and A. Catellani, Phys. Rev. B **53**, 4630 (1996), and references therein.

[13] R. Winkler, and A. I. Nesvizhskii, Phys. Rev. B **53**, 9984 (1996), and reference therein.

[14] Y. Tang, H. T. Lin, D. H. Rich, P. Colter, and S. M. Vernon, Phys. Rev. B **53**, R10 501 (1996).

[15] G. A. Baraff and D. Gershoni, Phys. Rev. B **43**, 4011 (1991).

[16] Yong Zhang, Phys. Rev. B **49**, 14 352 (1994).

[17] P. Dua, S. L. Cooper, A. C. Chen, and K. Y. Cheng, Appl. Phys. Lett. **69**, 2261 (1996).

[18] R. D. Twesten, J. Mirecki Millunchick, S. P. Ahrenkiel, Yong Zhang, S. R. Lee, D. M. Follstaedt, A. Mascarenhas, and E. D. Jones, in *Thin Films—Structure and Morphology*, edited by S. C. Moss, D. Iia, R. C. Cammarata, E. H. Chason, T. L. Einstein, and E. D. Williams, MRS Symposia Proceedings No. 441 (Materials Research Society, Pittsburgh, 1997), p. 187.
[19] J. Mirecki Millunchick, R. D. Twesten, S. R. Lee, D. M. Follstaedt, E. D. Jones, S. P. Ahrenkiel, Y. Zhang, H. M. Cheong, and A. Mascarenhas, J. Electron. Mater. **26**, 1048 (1997).
[20] E. D. Jones, J. Mirecki Millunchick, D. M. Follstaedt, M. Hafich, S. R. Lee, J. Reno, R. D. Twesten, Y. Zhang, and A. Mascarenhas, Proc. SPIE **2994**, 468 (1997).
[21] J. Mirecki Millunchick, R. D. Twesten, S. R. Lee, D. M. Follstaedt, E. D. Jones, S. P. Ahrenkiel, Y. Zhang, H. M. Cheong, and A. Mascarenhas, MRS Bull. **22**, 38 (1997).
[22] S.-H. Wei, L. G. Ferreira, J. E. Bernard, and A. Zunger, Phys. Rev. B **42**, 9622 (1990); S.-H. Wei (private communication).
[23] F. Glas, J. Appl. Phys. **62**, 3201 (1987).
[24] S.-H. Wei, D. B. Laks, and A. Zunger, Appl. Phys. Lett. **62**, 1937 (1993).
[25] S. R. Lee *et al.* (unpublished).
[26] C. Lugand, T. Benyattou, G. Guillot, T. Venet, M. Gendry, G. Hollinger, and B. Sermage, Appl. Phys. Lett. **70**, 3257 (1997); R. P. Schneider, Jr., R. P. Bryan, E. D. Jones, and J. A. Lott, *ibid.* **63**, 1240 (1993).
[27] C. Mailhiot and D. L. Smith, Cryst. Prop. Prep. **21**, 1 (1989).
[28] J. J. Hopfield, J. Phys. Chem. Solids **15**, 97 (1960).
[29] A. Eyal, R. Beserman, S. H. Wei, A. Zunger, E. Maayan, O. Kreinin, J. Salzman, R. Westphalen, and K. Heime, Jpn. J. Appl. Phys., Part 1 **32**, Suppl. 32-3, 716 (1993).
[30] G. Bastard, *Wave Mechanics Applied to Semiconductor Heterostructures* (Les Editions de Physique, Les Ulis Cedex, 1988).
[31] Y. C. Chang and J. N. Schulman, Phys. Rev. B **31**, 2069 (1985); Yong Zhang, A. Mascarenhas, P. Ernst, F. A. J. M. Driessen, D. J. Friedman, K. A. Bertness, J. M. Olson, C. Geng, F. Scholz, and H. Schweizer, J. Appl. Phys. **81**, 6365 (1997).
[32] A. Mascarenhas, Yong Zhang, J. Mirecki Millunchick, R. D. Twesten, and E. D. Jones, in *Proceedings of Future generation Photovoltaic Technologies: First NREL Conference*, edited by R. McConnell, AIP Conf. Proc. No. 404 (AIP, Woodbury, NY, 1997), p. 303.
[33] G. L. Bir and G. E. Pikus, *Symmetry and Strain-Induced Effects in Semiconductors* (Wiley, New York, 1974).
[34] T. B. Bahder, Phys. Rev. B **41**, 11 992 (1989); **46**, 9913 (1992).